Self-folded soft robotic structures with controllable joints

Self-folded Soft Robotic Structures with Controllable Joints

Cynthia Sung, Rhea Lin, Shuhei Miyashita, Sehyuk Yim, Sangbae Kim, and Daniela Rus

Abstract— **This paper describes additive self-folding, an origami-inspired rapid fabrication approach for creating actuatable compliant structures. Recent work in 3-D printing and other rapid fabrication processes have mostly focused on rigid objects or objects that can achieve small deformations. In contrast, soft robots often require elastic materials and large amounts of movement. Additive self-folding is a process that involves cutting slices of a 3-D object in a long strip and then pleat folding them into a likeness of the original model. The zigzag pattern for folding enables large bending movements that can be actuated and controlled. Gaps between slices in the folded model can be designed to provide larger deformations or higher shape accuracy. We advance existing planar fabrication and self-folding techniques to automate the fabrication process, enabling highly compliant structures with complex 3-D geometries to be designed and fabricated within a few hours. We describe this process in this paper and provide algorithms for converting 3-D meshes into additive self-folding designs. The designs can be rapidly instrumented for global control using magnetic fields or tendon-driven for local bending. We also describe how the resulting structures can be modeled and their responses to tendon-driven control predicted. We test our design and fabrication methods on three models (a bunny, a tuna fish, and a starfish) and demonstrate the method's potential for actuation by actuating the tuna fish and starfish models using tendons and magnetic control.**

I. Introduction

Recent advances in rapid fabrication technologies have significantly lowered the barrier to robot design and manufacturing, allowing complex mechanisms and 3-D structures to be created more easily than ever [1]. The main appeal of these 3-D printing approaches for robotic applications is that unlike with traditional manufacturing techniques, entire mechanisms can be created without requiring post-fabrication assembly [2]–[4], leading to fully printed robots that can be designed, fabricated, and deployed in a matter of only hours or days.

Unfortunately, most 3-D printing techniques target fabrication of rigid structures, and rapid fabrication methods for compliant mechanisms have been much more limited. Although multi-material printers exist for creating soft objects [5]–[8] and have been used for robot fabrication [9], the printed structures fail when experiencing large deformations. In contrast, soft or compliant robots frequently depend on highly elastic materials in order to perform [10]. As a result, creating these structures often involves multi-step fabrication and assembly processes [11], [12] whose complexity increases with the complexity of the device geometry.

C. Sung, R. Lin, and D. Rus are with the Computer Science and Artificial Intelligence Laboratory, Massachusetts Institute of Technology, Cambridge, MA, USA emails: {crsung, rhea, rus}@csail.mit.edu. S. Miyashita is with the Department of Electronics, University of York, York, UK email: shuhei.miyashita@york.ac.uk. S. Yim is with Robotics and Media Institute, Korea Institute of Science and Technology, Seoul, South Korea email: sehyuky@kist.re.kr. S. Kim is with the Department of Mechanical Engineering, Massachusetts Institute of Technology, Cambridge, MA, USA email: sangbae@mit.edu.

In this paper, we demonstrate a new technique that we call additive self-folding (ref. Fig. 1). This process involves creating long strips of material that are then self-folded into a pleated structure that can bend and deform similarly to existing soft actuators. The shapes of the strips are designed to produce a particular 3-D shape when folded in this way. Origami-inspired approaches have been proposed to replace [13]–[16] or enhance [17] soft structures before, but these patterns are often manually tuned for the application and are difficult to generalize to other geometries. In contrast, fabrication approaches that cut and paste together slices of 2-D material [18], [19] allow users to create general geometries but do not provide obvious modes of actuation and control. Additive self-folding combines the advantages of both approaches by producing structures that can be designed for complex 3-D geometries while providing potential for actuation.

Additive self-folding leverages an automated self-folding process in the vein of [20] that decreases human error during assembly. We also detail algorithms for automated design that convert a 3-D mesh into an additive self-folded structure. We demonstrate actuation and control of these structures using two approaches: global magnetic control and tendon-driven control similar to existing soft robotic systems [21]–[24]. Our main contributions include:

- a rapid fabrication technique that enables complex compliant structures to be self-assembled and actuated in a couple of hours with minimal human intervention,
- algorithms for designing and modeling structures fabricated using this technique,
- experimental verification through three fabricated static structures, and
- two end-to-end examples demonstrating design, fabrication, and actuation for additive self-folded models.

The paper is organized as follows. Section II details our additive self-folding fabrication process. Section III describes design algorithms used to convert a 3-D mesh into an additive self-folding design. Section IV describes our model for tendon-driven control. Section V contains static and actuated structures fabricated using our approach. Section VI concludes with discussion and future work.

II. Additive Self-Folding

In additive self-folding, 3-D structures are constructed as stacked 2-D slices. The slices are fabricated as a long strip

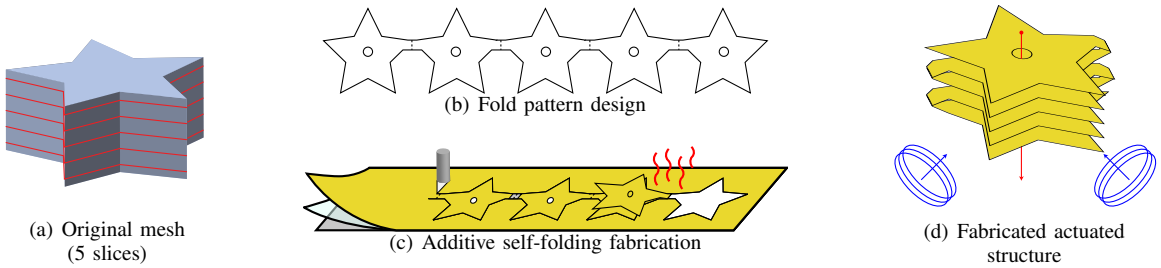

Fig. 1. Summary of additive self-folding design and fabrication approach for a star prism. (a) Inputted star prism mesh with 5 slices outlined. (b) Pleated fold pattern design generated from slices. The design is a strip with near-180° folds in alternating directions. (c) Additive self-folding fabrication process. The material consists of 3 layers that are cut and then self-folded using heat. (d) Fabricated model that can be actuated using tendons strung through holes (red) or magnetic coils (blue).

of flat material that is then self-folded with near-180° folds in alternating direction for alignment. When slices are folded so that they lie flat against each other, this procedure is able to produce solid 3-D objects at a resolution limited only by the thickness of the material used and the size of the fold. When slices are folded with gaps between them, the result is a compliant structure with the ability to bend and deform.

The folded strips of material are fabricated as a layered structure and heated to induce self-folding into the 3-D model. Our fabrication procedure advances that in [20] to provide streamlined fabrication and material layer alignment, as well as accelerated self-folding using a near-boiling water bath. In particular, the self-folding patterns are composed of a layer of shrinking material in between two layers of model material. Gaps are cut in the model material layers so that when the shrinking layer contracts, the entire structure will fold in the direction of the gap. In order to more precisely position folds, every gap is paired with a perforated cut in the model material layer on the other side.

The material layers are cut and aligned using the procedure shown in Fig. 2. First, a sheet of the model material is covered with double-sided adhesive, and gaps and perforations for both layers are cut out of it (Fig. 2(a)). A sheet of the shrinking material is then pressed onto the adhesive, and the model material is folded in half to align the two sides around the shrinking layer (Fig. 2(b)). The border of the model template is cut out from the resulting three layer material (Fig. 2(c)). In this work, DuraLar Mylar was used as the model material and PVC was used for the shrinking layer. The layers were attached to each other using silicone transfer tape. Each of the layers was 0.051 mm thick, resulting in a total material thickness of 0.27 mm. To fold the structures, the patterns were vertically lowered into near-boiling water (90°C is optimal for 180° folding with PVC). The heat transferred from the water causes the material to fold almost instantly. Weights were attached at the end of the pattern to ensure that it would sink.

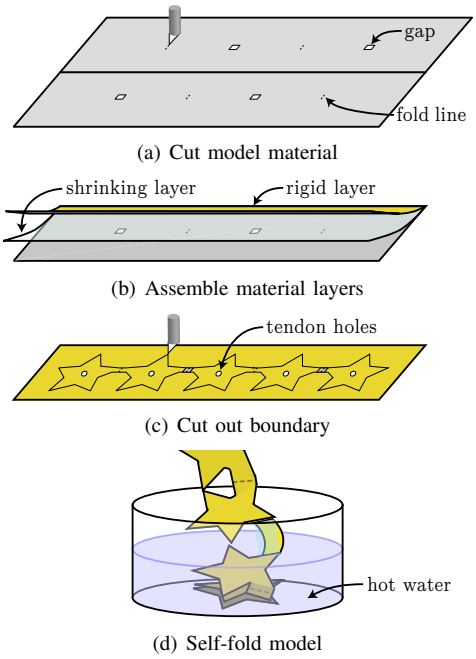

Fig. 2. Additive self-folding fabrication process. (a) Gaps and fold lines are cut into the model material. (b) The model material is aligned with a shrinking layer in the middle. (c) The boundary of the design is cut out of the three layers. (d) The design is self-folded in water.

III. Design Algorithms

The patterns for each of the layers in the fabrication process can be generated automatically from an inputted 3-D mesh. Our algorithm slices the mesh at a user-specified slice resolution and generates a fold pattern corresponding to the pleat-folded structure. The slice resolution, that is, the distance between slices of material, controls the compliance and actuation potential of the fabricated structure (see Section IV for more details). The resulting fold pattern is then converted into a self-folding design by determining what material cuts will result in the necessary fold angles to achieve the given slice resolution.

A. Pleated Fold Pattern Design

The fold pattern design is constructed using Alg. 1. The algorithm takes as input a 3-D mesh and a slice resolution. It then slices the mesh and computes fold locations. The directions of slicing and folding can be chosen arbitrarily for a given mesh, as long as they are orthogonal to each other. In the following discussion, we will assume that the slicing occurs in the $\mathbf{z}$ direction and folds are placed in the $\mathbf{x}$ direction, as shown in Fig. 3.

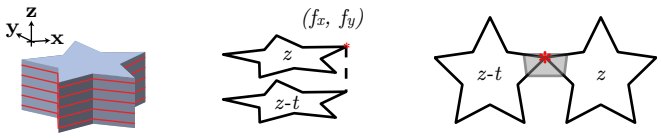

(a) 3-D mesh (b) Fold location (c) Resulting unfolding

Fig. 3. The SLICE3D algorithm (a) slices an inputted mesh in the **z** direction and (b) locates folds at the extreme x coordinate of adjacent slices. The result is expanded into an unfolding (c). The gray material is added to the fold.

The algorithm starts with the minimum z value for the mesh and iteratively processes slices at increasing z values until it slices the entire model. Depending on the complexity of the model, it is possible that individual slices may contain multiple disconnected polygon components. Therefore, for each of the polygon components, the algorithm locates folds connecting it to the previous slice (lines 11–14). The algorithm alternates between placing folds in the $+x$ and $-x$ direction to correspond to the pleated structure. In order to prevent faces from intersecting in the fold pattern design, the folds are placed at the maximum or minimum x values of the entire slices at the current and previous z value (lines 5–9).

Since folds have some length and are necessarily straight, adding folds to the structure will change the geometry of the 3-D model. We choose to strictly add material to the geometry, and we therefore center the fold at a y coordinate that minimizes the amount of material added (line 11). This value f_y is required to be within the minimum and maximum y coordinates of the polygon p_z^i being processed and is computed as the y value that produces the minimum sum of distances to the boundary of p_z^i and $Slice_{z-t}$.

Once the connectivity of the fold pattern has been determined, holes for tendons can be added to the structure for actuation (line 17; ref. Section IV). The slices are then transformed according to the fold locations, and creases are added to complete the fold pattern (lines 18–19).

1) Optimizations: Algorithm 1 states the folds are placed at the extreme x coordinates of the slices being connected, even if the resulting f_x coordinate is far away from the slice boundaries at the computed f_y value. This choice ensures that branches of material originating from multiple polygons in a slice do not produce fold patterns that intersect. However, it also produces extra material that changes the 3-D geometry and is not always necessary. The added material can be reduced in a post-processing step that shifts faces in the fold pattern to bring folds as close as possible to the slice boundaries while keeping the pattern non-self-intersecting.

2) Achievable Geometries: The outlined procedure is ideally suited for 3-D objects with only one polygon component per slice. In this case, the accuracy of the fabrication process depends on the size of the folds compared to the slope of slice boundaries. As described, the algorithm is able to handle geometries with disconnected slices, but its success will depend on the slicing and folding directions and the arrangement of the polygon components (ref. Fig. 4), and it

Algorithm 1: SLICE3D$(\mathcal{M}, t)$

Input: A mesh $\mathcal{M}$, slice height t

```
// Extract connectivity graph
```
1 $\mathcal{P} \leftarrow \emptyset$; // polygonal faces
2 $\mathcal{F} \leftarrow \emptyset$; // fold connections
3 **for** $z = z_{min}$ **to** z_{max} **step** t **do**
4 $Slice_z \leftarrow$ slice of $\mathcal{M}$ at z;
5 **if** $Slice_z$ *is an even-numbered slice* **then**
6 $f_x \leftarrow$ max x coordinate of $Slice_{z-t}$ and $Slice_z$;
7 **else**
8 $f_x \leftarrow$ min x coordinate of $Slice_{z-t}$ and $Slice_z$;
9 **end**
10 **foreach** *simple polygon* p_z^i *in* $Slice_z$ **do**
11 $f_y \leftarrow y$ value yielding minimum added material for a fold at f_x attached to p_z^i and $Slice_{z-t}$;
12 $p_{z-t}^j \leftarrow$ polygon in $Slice_{z-t}$ corresponding to computed f_y;
13 Add p_z^i to $\mathcal{P}$;
14 Add $\left(p_{z-t}^j, p_z^i, (f_x, f_y)\right)$ connection to $\mathcal{F}$;
15 **end**
16 **end**
17 Place tendons if desired;
18 Unfold faces in $\mathcal{P}$ at fold connections in $\mathcal{F}$;
19 Add extra material and creases to connect face material;

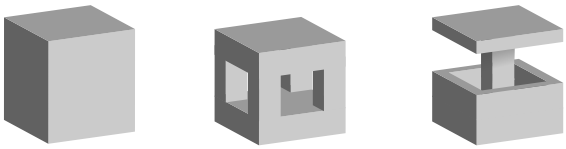

(a) Achievable (b) Achievable (c) Non-achievable

Fig. 4. Achievable and non-achievable geometries using the SLICE3D algorithm. (a) Geometry where every slice is a single component. (b) Geometry with multiple component polygons in middle slices that can have branching structure. (c) Geometry with a hole that cannot be achieved because the pillar in middle would always be disconnected.

may result in merging polygons for certain arrangements. Provided no polygons are enclosed by other polygons, it is possible to choose new folding directions to produce a branching structure where each polygon component spawns a fold pattern extending in a different direction. This procedure increases the likelihood that disconnected polygons in a slice will remain disconnected, though the error in the 3-D geometry will still depend on the size of the folds compared to the model.

B. Self-Folding Pattern

The fold pattern is converted into a self-folding design by adding gaps and perforations into the pattern and separating the cuts for the different layers of material.

First, the size of the fold lines and gaps required to achieve the desired slice height are computed. To determine

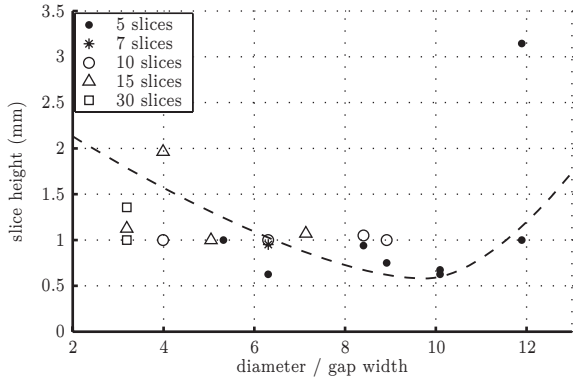

(a) Slice height vs relative face width

(b) Additive self-folded cylinders tested

Fig. 5. Resulting slice height for additive self-folded cylinders. (a) Plot of slice height data compared to the ratio of face diameter to gap width. (b) Sample cylinders with diameter 15 mm and 4 mm × 4 mm gaps for 5, 7, and 10 slices.

the required gap dimensions $w_g \times w_g$, we collected slice height data for additive self-folded cylinders using a variety of cylinder and gap dimensions. The data is summarized in Fig. 5. The dotted line shows the trendline that we used for gap size computations. We found that the slice height after self-folding was mainly dependent on the ratio between the cylinder diameter and the gap width. Although theoretically only the exposed shrinking material contributes to folding, in practice the unexposed shrinking material between the rigid faces also shrinks slightly. Thus, larger ratios of face width to gap width lead to greater fold angles and smaller slice heights. The data also showed a large variation in slice height for large ratios of diameter to gap width, which we suspect comes from the increased resistance of the water on faces with larger surface area.

Once the required gap width is found, square gaps and perforations of this size are placed at each of the fold locations. The gaps are placed on the top and bottom model material layers in alternating order to induce the pleat folding. This procedure results in the cut lines required for the model and shrinking layers.

IV. Tendon-Driven Control

The slice resolution of the folded structure determines the accuracy of the final fabricated 3-D shape and its compliance. Designing a model with slice height greater than the material thickness results in a structure with air gaps. Because of the flexibility of the materials used at the creases during fabrication, the slices of the structure have the ability to collapse under force. Smaller gaps between slices help the entire structure to maintain a shape close to that of the

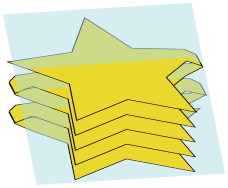

(a) Plane of motion

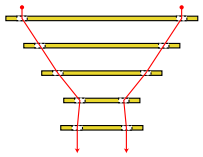

(b) Slice holes

Fig. 6. Locating tendon holes for bending in a plane. (a) To make the structure bend in a plane, take the intersection of the folded structure with the plane (light blue). (b) Tendons for motion are placed at the outer edges of the lines of intersection.

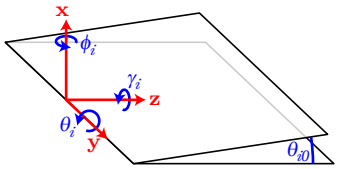

(a) Plane of motion

Fig. 7. Folds are modeled as 3 rotational springs centered on the fold.

selected mesh, while larger gaps allow greater deformations to occur. We leverage these deformations to create soft robotic devices by stringing tendons through the structure to control its movement. The locations of the tendons can be controlled to produce particular bending and twisting motions and to achieve both local and global deformations.

A. Tendon Placement

Bending in a plane for a model can be achieved by placing holes in the extreme locations of the slices (Fig. 6). For example, for bending in the **xz** plane, we find a cross-section of the 3-D model with a plane $y = y_0$. The intersection of each of the slices onto that plane is a line. We place two holes on the intersection line for each slice 2 mm away from the boundary of the slice. Placing the holes on both sides of the slice allows us to locate antagonistic tendons so that the model can bend in both directions.

In some cases, a slice will not intersect with the desired cross-sectional plane. In this case, a new plane that does intersect with the slice can be found, the closest point on the slice can be used, or the slice can be skipped altogether. We make the choice between these options by checking whether the distance of the slice boundary from the cross-sectional plane is within a distance threshold.

B. Pseudo-Rigid-Body Model

Because the connective folds between slices are relatively small compared to the faces themselves, we can model the folded structure as rigid faces connected by deformable joints. This assumption is commonly used when modeling folded structures [25], [26] and allows us to simplify analysis by ignoring deformations in the faces themselves.

We model each of the folds as three rotational springs centered at the center of the fold. Define a coordinate system on fold i where the **y** axis lies along the fold, the **z** axis lies

in the slice direction, and the $\mathbf{x}$ axis is defined according to right-hand convention (ref. Fig. 7). Then let θ_i, ϕ_i, and γ_i be the relative rotation of two faces connected by fold i about the $\mathbf{y}$, $\mathbf{x}$, and $\mathbf{z}$ axes respectively. As shown in [26], [27], folds can be modeled as linear springs provided the change in fold angle is small. Since this is the case for an additive self-folded model, we model the spring whose axis of rotation lies on the fold line, aligned with the $\mathbf{y}$ axis, as a linear spring with spring constant k_θ and equilibrium position equal to the fold angle θ_i that produces the user-specified slice height. Similarly, the springs producing restoring torques in ϕ_i and γ_i are also modeled as linear springs with spring constants k_ϕ and k_γ, respectively, and equilibrium positions at $\phi_i = 0$ and $\gamma_i = 0$. Since we use the same gap widths and fold lengths throughout the entire self-folding pattern, we can make the assumption that the stiffnesses k_θ, k_ϕ, and k_γ are constant over all the slices. Furthermore, since bending stiffness varies with wt^3, where w is the width of the bending material and t is the thickness, we can make the approximation that the stiffnesses k_ϕ and k_γ are a factor of w_g^2/t^2 greater than the stiffness k_θ.

Then the total spring potential energy stored in an additive self-folded structure is

$$E = \sum_{i}^{N_f} \left[\frac{k_\theta}{2} \left(\theta_i - \theta_{i0}\right)^2 + \frac{k_\phi}{2}\phi_i^2 + \frac{k_\gamma}{2}\gamma_i^2 \right] \qquad (1)$$

where N_f is the total number of folds in the structure, θ_i, ϕ_i, and γ_i are the angles at fold i, and θ_{i0} is the equilibrium fold angle of fold i.

Finally, we assume a frictionless tendon. In this case, the tendons act as length constraints on the folded model, and the model will converge to the lowest energy configuration that satisfies these constraints. Therefore, given tendon hole locations and lengths, we can compute the expected shape of an additive self-folded model as a convex optimization problem, or, assuming that tendons are being pulled and released continuously, using gradient descent.

V. Results

We have implemented our design algorithms in an interactive user interface (UI) that allows users to design an additive self-folded model starting from a 3-D mesh. The UI allows the users to choose the slice height and tendon locations for the given mesh and automatically outputs the additive self-folded design. Before fabrication, the user can test the design by virtually pulling on tendons and visualizing the resulting geometry.

A. Self-Folded 3-D Structures

We first tested our basic design and fabrication approach by creating three solid 3-D objects: a bunny, a tuna fish, and a starfish. In order to create a solid object, the slices and gaps were generated using a desired slice height equal to the total thickness of the material (0.27 mm). The designs were cut using a Silhouette Cameo vinyl cutter. Since the cutter uses a cutting mat of limited length, the bunny pattern was split into 3 parts during cutting and joined together with tape before self-folding. This constraint could be relaxed by using a cutter with autofeed functionality.

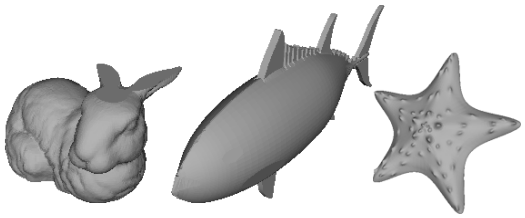

(a) 3-D meshes

(b) Fabricated models

Model	Slices	width (mm)		length (mm)		height (mm)	
		exp.	meas.	exp.	meas.	exp.	meas.
bunny	40	40.0	40	28.6	28	10.8	17
tuna	19	74.0	75	35.5	35	5.13	5
starfish	5	28.6	30	30.0	30	1.4	3

(c) Dimension comparison

Fig. 8. Static 3-D structures produced through additive self-folding: bunny, tuna fish, and starfish. (a) 3-D meshes used to generate designs. (b) Fabricated models. (c) Comparison of expected and measured dimensions.

Figure 8 shows the resulting models as compared to the inputted mesh. The models had well-aligned slices and their 3-D shapes bore close resemblances to the goal structures. Table 8(c) shows the number of slices and the dimensions of each model. Since the slicing of the models occurred in the height direction, we expect the measured widths and lengths to be very close to the expected values. This was the case for all three fabricated models. Differences in dimensions may be attributed to the extra material added at folds. The heights of the three models were fairly close to the expected heights but did show greater variation than the widths and lengths. In particular, the starfish was almost two times as tall as the expected height, indicating that the folds did not reach 180°. This error can be seen in the slice separation in the fabricated model.

Each of the models was fabricated in less than 30 min. Figure 9 shows snapshots of the self-folding process for the tuna and bunny models. Time required for self-folding was under 5 s for the starfish, 8 s for the tuna, and 22 s for the bunny, showing that this method is significantly faster than many existing self-assembly methods. Longer patterns with more slices tended to have longer folding time. All of the models self-folded at every fold location with near-180° folds. During experiments, we found that a key factor to complete folding was the alignment of the strip as it entered

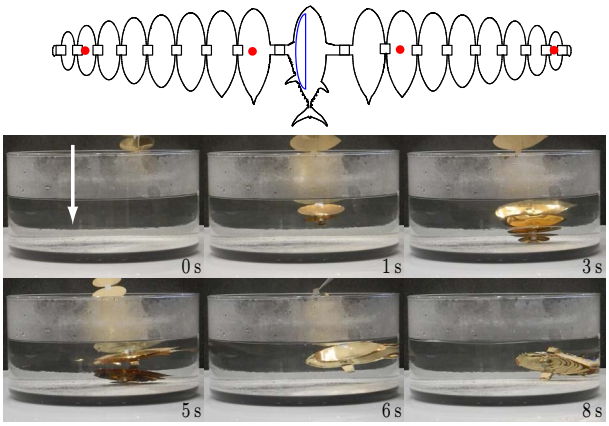

(a) Tuna fish

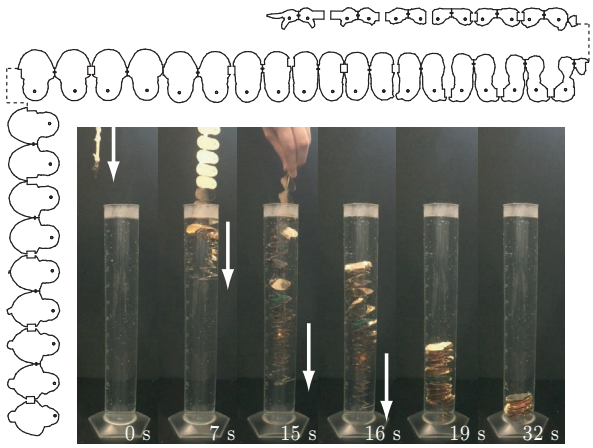

(b) Bunny

Fig. 9. Time lapse images taken during the (a) tuna fish and (b) bunny self-folding experiments, with fold patterns. In (a), red dots indicate magnets placed on the pattern before self-folding, and the blue half-ellipse was foam sheet added for floating.

the water. Long patterns such as the bunny tended to twist in the water if the container was too large. Using a narrower container such as a graduated cylinder helped with these alignment issues. All models maintained their shape after being removed from the water.

B. Global Actuation

The self-folded structures can be instantly actuated by a magnetic field by placing a permanent magnet inside the structure. We chose the tuna fish model to demonstrate this capability. Below the beaker of water used for self-folding, we placed four electromagnetic coils angled at 45° toward the center of the operational area in a manner similar to [20]. Four small cylindrical neodymium magnets (magnetic flux density 330 mT on the surface) were attached to the fish pattern before the self-folding process (ref. Fig. 9(a)). The magnets were fixed so that their poles lay perpendicular to the intended direction of movement. In addition, half of a 40 mm × 20mm ellipse of adhesive-backed foam was attached to each side of the centermost face of the flat fold pattern to keep the fish afloat after folding.

Fig. 10. Frames of the self-folded fish swimming in a water tank under magnetic control

Fig. 10 shows frames of the resulting movement when a magnetic field is applied by the coil setup. The produced magnetic field of 0.6 mT was alternated about the vertical axis by 45° at 2 Hz. As a result, the tuna fish model oscillates in the water and produces thrust to swim toward the aimed direction. Actuation is possible within seconds of the structure completing the self-folding process.

C. Local Actuation

In addition to global movements using an embedded magnet and magnetic field, we demonstrated tendon-driven control when the fabricated structures are not solid. All of our models were placed on a platform with holes. Fishing line 0.2 mm in diameter was threaded through the holes in the structure and the platform and actuated using Turnigy TGY-1370A servomotors controlled by an Arduino Uno. For this setup, our UI allows users to designate the servomotor connections and control the additive self-folded device by pulling the virtual tendons. The UI sends serial commands to the Arduino to execute the movements. We show the resulting model and motions for a single starfish leg and a full model with 5 legs.

Figure 11 shows a single leg of the starfish model and some of the resulting deformations. The leg was enlarged to 32.5 mm × 32.7 mm × 20.9 mm and sliced in the outward direction. The fold pattern was designed to a slice height of 0.56 mm, producing a total of 58 slices. The entire fabrication process took 72 min. to construct the layered material and 32 s to self-fold. The model was actuated using six tendons that produced forward, backward, left, and right bending motions, and a twisting motion about the **z** direction.

The leg was able to achieve all the intended bending motions. In order to demonstrate how local motions could be produced, we split the right bending motion into bending in the top half of the leg and bending at the bottom. These motions can be combined to produce more interesting motions, such as for the leg bending left with a rightward bending top in Fig. 11(f). Loosening tendons removes the distance constraint and should allow the natural elasticity of the leg to bring the structure back to its neutral position. In practice, friction between the tendon and the layers often prevented the structure from recovering completely. As a result, pulling on the tendon on the opposite side of the structure was necessary to return the structure to neutral state.

During bending, the leg experienced a maximum decrease in length of 29.5%. This value is much less than the theoretical value of $\frac{0.56\text{ mm}-0.27\text{ mm}}{0.56\text{ mm}} = 51.8\%$. This is because folds in models with large slice gaps, unlike the ones for the compact structures in the previous sections, are curves

(a) Neutral (b) Bend forward (c) Bend backward

(d) Bend left (e) Bend right (f) Bend left, right top

Fig. 11. Movements by tendon-driven model of a single starfish leg fabricated using additive self-folding

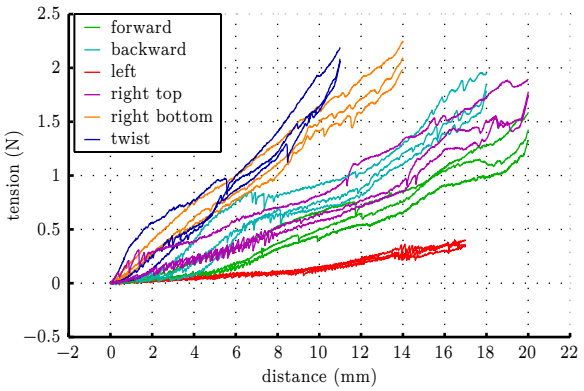

Fig. 12. Measured tendon tension for each tendon in the starfish leg

rather than crisp folds. To see whether this difference affects our model, we measured the force required to pull each of the tendons in the structure on an Instron 5944 machine. Figure 12 shows the resulting measurements for 3 instances of pulling each tendon starting from the leg's neutral state. Tendon tensions were approximately linear, confirming the validity of our model assumptions. Jumps in measured force occurred when tendons caught on holes in the platform.

Finally, we constructed a complete starfish model by fabricating 5 of the single legs. In this case, each of the legs was driven by 4 tendons producing bending in the up, down, left, and right directions. The completed starfish was 88.3 mm $\times$ 84.3 mm $\times$ 26.5 mm in size. Each leg took about 50 min. to fabricate. Figure 13 shows the result.

To demonstrate group motion, we controlled the starfish using 6 servomotors to control 1) clockwise bending of all the legs, 2) counterclockwise bending of all the legs, 3) upward bending of 2 legs, 4) downward bending of 2 legs, 5) upward bending of 3 legs, and 6) downward bending of 3 legs. Because each of the legs is strung with its own tendon, the lengths of each of the tendons had to be carefully calibrated in order to ensure leg groups moved synchronously. In addition, gravity caused the parts of the legs extending past the end of the platform to bend downward. As a result downward bending produced more of a contracting effect than a bending motion. Tightening the tendons for upward bending in the legs mitigated this effect.

VI. Discussion

In this paper, we demonstrate additive self-folding fabrication, a method for rapidly producing compliant structures with a wide range of 3-D geometries. We have outlined our fabrication approach, which enables full 3-D structures to be fabricated with minimal human intervention, and we have provided algorithms for automatically generating the fabrication plans for a given 3-D shape. We have modeled the resulting structures, showing that it is possible to predict the kinematics of the self-folded structures and to control their movement. We have demonstrated our methods through 3 static geometries and 3 actuated designs.

Our results demonstrate the use of origami-inspired approaches to accelerate the design, fabrication, and actuation of compliant structures. The methods are fast, requiring only a few hours to go from 3-D mesh to fabricated prototype, and they require few manual assembly steps. In fact, the most labor-intensive part of fabricating our tendon-actuated models was stringing the tendons through the folded structure, a process that took almost as long as the rest of the fabrication process combined. Integrating the actuation method into the layered self-folding material would simplify fabrication.

Other limitations for our process include the materials used and the achievable sizes for fabricated structures. Our models rely on fold stiffness for bending. However, in large structures, the weight may cause the folds to collapse, meaning that only solid structures can realistically be made. Investigating other materials or patterns that can be used for structures larger than the centimeter scale are needed. In addition, friction between the tendons and the faces affected control for the tendon-driven models. Our experiments show linear required tension forces, indicating that friction may be able to be lumped into the stiffness parameters, but further investigation into the friction model is also needed.

Finally, the greatest limitation of our fabrication approach is the range of achievable geometries. Although we have shown that we are able to produce a wide variety of shapes, our design algorithms provide little guidance for structures containing multiple holes or branches. As shown for the actuated starfish, it is possible to cut a mesh into multiple parts and individually fabricate them depending on the geometry and actuation goals. Future work includes determining when and how to cut a mesh so that structures of greater complexity and capabilities can be produced.

Acknowledgments

Support for this project has been provided in part by NSF Grant Nos. 1240383 and 1138967. We thank Jeffrey Lipton and Robert Katzschmann for their constructive feedback, and Emily Southern and Valerie Bugmann for their assistance in fabricating the models.

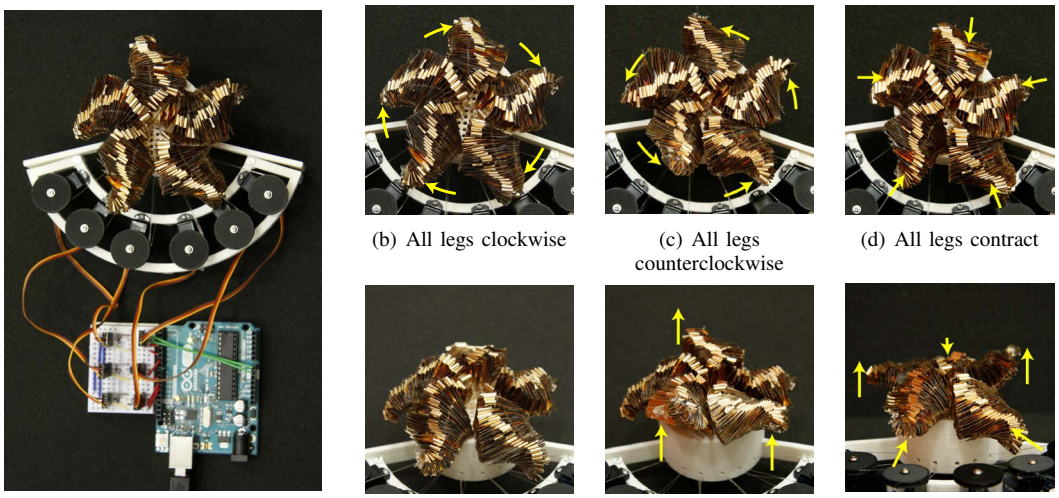

(a) Experimental setup (b) All legs clockwise (c) All legs counterclockwise (d) All legs contract (e) Starfish, side view (f) 3 legs up (g) 2 legs up, 3 legs contract

Fig. 13. Full starfish model fabricated using additive-self folding. (a) Experimental setup containing fabricated model and tendons controlled by servomotors. (b)-(g) Movements achievable by starfish.

REFERENCES

[1] W. Gao, Y. Zhang, D. Ramanujan, K. Ramani, Y. Chen, C. B. Williams, C. C. L. Wang, Y. C. Shin, S. Zhang, and P. D. Zavattier, "The status, challenges, and future of additive manufacturing in engineering," *Computer-Aided Design*, vol. 69, pp. 65–89, 2015.

[2] C. Mavroidis, K. J. DeLaurentis, J. Won, and M. Alam, "Fabrication of non-assembly mechanisms and robotic systems using rapid prototyping," *ASME Journal of Mechanical Design*, pp. 516–524, 2000.

[3] J. Calì, D. A. Calian, C. Amati, R. Kleinberger, A. Steed, J. Kautz, and T. Weyrich, "3D-printing of non-assembly, articulated models," *ACM Transactions on Graphics*, vol. 31, no. 6, p. 130, 2012.

[4] M. Fuge, G. Carmean, J. Cornelius, and R. Elder, "The MechProcessor: Helping novices design printable mechanisms across different printers," *Journal of Mechanical Design*, vol. 137, no. 11, p. 111415, 2015.

[5] P. Huang, D. Deng, and Y. Chen, "Modeling and fabrication of heterogeneous three-dimensional objects based on additive manufacturing," in *Proceedings of the ASME International Mechanical Engineering Congress and Exposition*, 2013, pp. IMECE2013–65 724.

[6] P. Sitthi-Amorn, J. E. Ramos, Y. Wangy, J. Kwan, J. Lan, W. Wang, and W. Matusik, "Multifab: A machine vision assisted platform for multi-material 3d printing," *ACM Transactions on Graphics*, vol. 34, no. 4, p. 129, 2015.

[7] "Connex3 - rapid tooling and prototyping in multiple materials," 2016. [Online]. Available: http://www.stratasys.com/3d-printers/production-series/connex3-systems

[8] M. Wehner, R. L. Truby, D. J. Fitzgerald, B. Mosadegh, G. M. Whitesides, J. A. Lewis, and R. J. Wood, "An integrated design and fabrication strategy for entirely soft, autonomous robots," *Nature*, vol. 536, pp. 451–466, 2016.

[9] V. Vikas, E. Cohen, R. Grassi, C. Sözer, and B. Trimmer, "Design and locomotion control of soft robot using friction manipulation and motor-tendon actuation," *IEEE Transactions on Robotics*, vol. 32, no. 4, pp. 949–959, 2015.

[10] D. Rus and M. T. Tolley, "Design, fabrication and control of soft robots," *Nature*, vol. 521, no. 7553, pp. 467–475, 2015.

[11] M. T. Tolley, R. F. Shepherd, M. Karpelson, N. W. Bartlett, K. C. Galloway, M. Wehner, R. Nunes, G. M. Whitesides, and R. J. Wood, "An untethered jumping soft robot," in *Proc. of IEEE/RSJ Intl. Conf. on Intelligent Robots and Systems*, 2014, pp. 561–566.

[12] R. K. Katzschmann, A. D. Marchese, and D. Rus, "Hydraulic autonomous soft robotic fish for 3D swimming," in *Experimental Robotics*, 2016, pp. 405–420.

[13] K. Zhang, C. Qiu, and J. S. Dai, "An extensible continuum robot with integrated origami parallel modules," *ASME Journal of Mechanisms and Robotics*, vol. 8, no. 3, p. 031010, 2016.

[14] C. D. Onal, R. J. Wood, and D. Rus, "An origami-inspired approach to worm robots," *IEEE/ASME Transactions on Mechatronics*, vol. 18, no. 2, pp. 430–438, 2013.

[15] B. A. Jones and I. D. Walker, "Kinematics for multisection continuum robots," *IEEE Transactions on Robotics*, vol. 22, no. 1, pp. 43–55, 2006.

[16] W. McMahan, B. A. Jones, and I. D. Walker, "Design and implementation of a multi-section continuum robot: Air-octor," in *Proc. of IEEE/RSJ Intl. Conf. on Intelligent Robots and Systems*, 2005, pp. 2578–2585.

[17] R. V. Martinez, C. R. Fish, X. Chen, and G. M. Whitesides, "Elastomeric origami: Programmable paper-elastomer composites as pneumatic actuators," *Advanced Functional Materials*, vol. 22, no. 7, pp. 1376–1384, 2012.

[18] H. Peng, J. Mankoff, S. E. Hudson, and J. McCann, "A layered fabric 3D printer for soft interactive objects," in *Proc. of 33rd Annual ACM Conference on Human Factors in Computing Systems*, 2015, pp. 1789–1798.

[19] "3D printing and rapid prototyping — Mcor Technologies," 2015. [Online]. Available: http://mcortechnologies.com/

[20] S. Miyashita, S. Guitron, M. Ludersdorfer, C. R. Sung, and D. Rus, "An untethered miniature origami robot that self-folds, walks, swims, and degrades," in *Proc. of IEEE Intl. Conf. on Robotics and Automation (ICRA)*, 2015, pp. 1490–1496.

[21] A. M. Dollar and R. D. Howe, "The highly adaptive SDM hand: Design and performance evaluation," *International Journal of Robotics Research*, vol. 29, no. 5, pp. 585–597, 2010.

[22] M. Cianchetti, A. Arienti, M. Follador, B. Mazzolai, P. Dario, and C. Laschi, "Design concept and validation of a robotic arm inspired by the octopus," *Materials Science and Engineering: C*, vol. 31, no. 6, pp. 1230–1239, 2011.

[23] C. Laschi, M. Cianchetti, B. Mazzolai, L. Margheri, M. Follador, and P. Dario, "Soft robot arm inspired by the octopus," *Advanced Robotics*, vol. 26, no. 7, pp. 709–727, 2012.

[24] A. Stilli, H. A. Wurdemann, and K. Althoefer, "Shrinkable, stiffness-controllable soft manipulator based on a bio-inspired antagonistic actuation principle," in *Proc. of IEEE/RSJ Intl. Conf. on Intelligent Robots and Systems (IROS)*, 2014, pp. 2476–2481.

[25] L. L. Howell, *Compliant mechanisms*. New York, NY, USA: John Wiley & Sons, 2001.

[26] C. Qiu, V. Aminzadeh, and J. S. Dai, "Kinematic analysis and stiffness validation of origami cartons," *ASME Journal of Mechanical Design*, vol. 135, no. 11, p. 111004, 2013.

[27] C. Sung and D. Rus, "Foldable joints for foldable robots," *ASME Journal of Mechanisms and Robotics*, vol. 7, no. 2, p. 021012, 2015.